THE JOURNAL OF PHYSICAL CHEMISTRY C

Article

pubs.acs.org/JPCC

Comparison of Charge-Transfer Dynamics of Naphthalenediimide Triads in Solution and π-Stack Architectures on Solid Surfaces

Oleksandr Yushchenko, Diego Villamaina, Naomi Sakai, Stefan Matile,* and Eric Vauthey*

School of Chemistry and Biochemistry, University of Geneva, 30 Quai Ernest Ansermet, CH-1211 Geneva 4, Switzerland

Supporting Information

ABSTRACT: The femto- to microsecond excited-state dynamics of an electron donor−acceptor−donor triad, consisting of two red core-substituted naphthalenediimides (rNDI) and one colorless naphthalenediimide (pNDI), in solution has been compared to that of a supramolecular surface architecture, constituted of coaxial stacks of rNDI and pNDI and prepared by self-organizing surface initiated polymerization (SOSIP). In the triad, charge separation between an excited rNDI and pNDI takes place in highly polar solvents only and for a subensemble of molecules, around 30%, with a folded conformation. Other processes, such as singlet and triplet excitation energy transfer from pNDI to rNDI and intersystem crossing, are also operative. Additionally, bimolecular symmetry-breaking charge separation upon triplet−triplet annihilation is observed on the microsecond time scale in polar solvent. In the surface architecture, excitation of an rNDI is followed by an ultrafast symmetry breaking-charge separation resulting in a charge-transfer exciton, which either recombines or dissociates into a charge-separated state with the electron and the hole in different stacks. The same charge-separated state can also be populated upon excitation of pNDI, either via a charge-transfer pNDI exciton or after excitation energy transfer to rNDI. Charge recombination in the SOSIP film takes place on a wide range of time scales, ranging from a few picoseconds to several hundreds of microseconds.

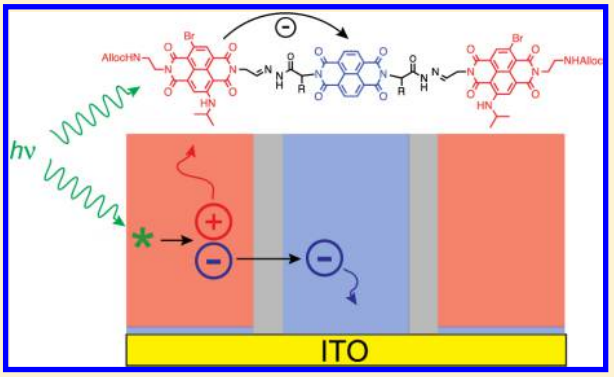

INTRODUCTION

Over the past decades, important efforts have been invested in the design of elaborate molecular architectures containing many chromophoric units for various applications, such as solar energy conversion, artificial photosynthesis, or molecular electronics.[1−11] A large number of chromophores is advantageous for increasing the absorption cross-section, but too high a density augments the mutual interactions and considerably changes the photophysical properties. In natural systems, this problem is prevented by the proteinic scaffold, which holds the pigments at distances and/or orientations that keep coupling small but sufficient to enable excitation energy and/or charge transfer.[12−14] These systems have been optimized through natural selection, a tool that is not available for synthesizing artificial mimics. Consequently, synthetic supramolecular architectures comprising a large number of chromophores (>10−20) are usually based on self-assembly.[3−5,11,15,16] The latter often rely on π−π and dispersion interactions, and, as a consequence, the chromophores are rather densely packed, like in aggregates. In this case, excitonic interaction often results in a delocalized excitation and a splitting of the electronic energy levels that may lead to a rapid quenching or to other properties than those originally anticipated. Whereas these effects are well understood with simple dyes,[17−20] less is known when the constituting bricks are themselves composed of several chromophoric units, such as electron donor−acceptor (D−A) polyads. The excited-state properties of these polyads are generally determined in solution phase, in general in polar solvents to favor charge-transfer processes.[21−26] However, in practical devices, these polyads have often to be organized in rigid structures, where substantial interactions with nearby polyads can take place and where the local environment differs strongly from that in solution phases. As a consequence, significant differences in the photophysical properties and performances can be expected.

We present here a comparative investigation of the excited-state dynamics of a D−A−D triad in solution and of solid films, consisting of parallel and alternating π stacks of donors and acceptors, prepared by self-organized surface-initiated polymerization (SOSIP) on an ITO-covered transparent surface and stack exchange (Figure 1).[10,27] Both D and A are naphthalenediimide (NDI) chromophores: A is substituted on the N atoms only, is colorless with absorption below 400 nm, and will be called further p(ale)NDI; D is additionally substituted at the naphthalene core with an amino group and a Br atom, is red colored,[28] and will be abbreviated r(ed)NDI. The SOSIP systems produce photocurrent when used as a working electrode in the presence of a mobile electron donor

Received: April 28, 2015
Revised: June 4, 2015
Published: June 5, 2015

DOI: 10.1021/acs.jpcc.5b04060
J. Phys. Chem. C 2015, 119, 14999−15008

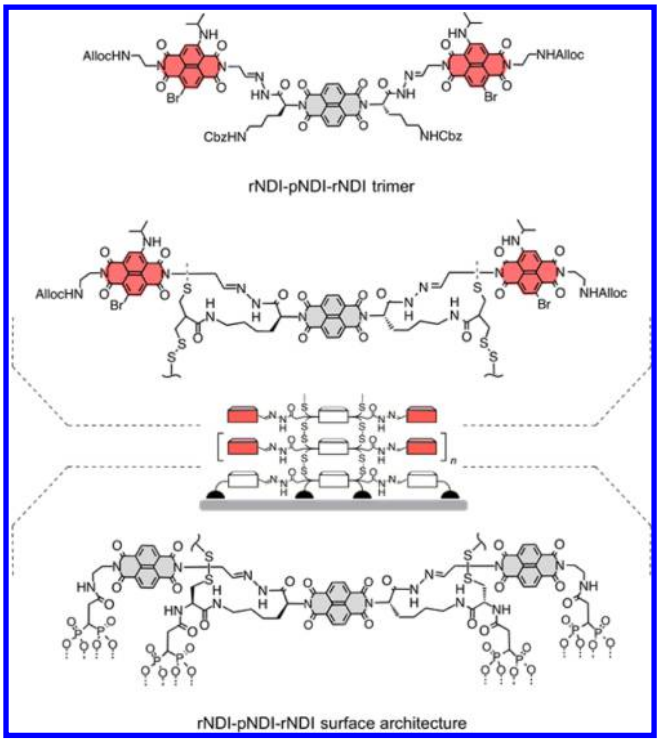

Figure 1. Structure of rNDI−pNDI−rNDI surface (SOSIP) architecture as compared to the rNDI−pNDI−rNDI trimer in solution ($n \approx 180$; rNDIs contain both 2,6- and 3,7-substituted isomers).

and a counter electrode.[27] Photocurrent can also be generated with surface architectures based on a single chromophore, such as a yellow naphthalenediimide. Ultrafast spectroscopic measurements on such a single-channel system have revealed that the origin of the photocurrent is photoinduced symmetry-breaking charge separation within a π stack.[10] The double-channel SOSIP system investigated here with parallel D and A stacks should function as a supramolecular n/p-heterojunction and should have superior performance.[27]

To understand the origin of the photocurrent in the surface architecture, we have performed time-resolved spectroscopic measurements on this system as well as on the triad in solution. As the linkers between the pNDI and rNDI units are the same for the trimer and the SOSIP architecture, the effect of the transition from dilute solution phase to dense packing on the excited-state dynamics can be directly evidenced.

EXPERIMENTAL SECTION

Samples. The rNDI−pNDI−rNDI surface architecture was prepared by SOSIP and stack exchange as described in ref 27. For the spectroscopic measurements, 3 × 3 cm^2 transparent ITO electrodes covered with a ∼60 nm thick SOSIP film were used. The synthesis of the rNDI−pNDI−rNDI trimer is described in the Supporting Information. All measurements with the trimer were performed in acetonitrile (ACN, Fisher Scientific, analytical grade) and dichloromethane (DCM, Fisher Scientific, analytical grade).

Steady-State Spectroscopy. Absorption spectra were measured on a Cary 50 spectrometer, whereas fluorescence emission and excitation spectra were recorded on a FluoroMax-4 (Horiba Scientific) fluorometer. All emission spectra were corrected for the wavelength dependence sensitivity of the detector.

Time-Resolved Fluorescence. Fluorescence dynamics on the nanosecond time-scale was measured using a time-correlated single photon counting (TCSPC) setup described in detail previously.[29,30] Excitation was performed at 469 nm using ∼60 ps pulses at 10 MHz produced by laser diodes (Picoquant, LDH-PC-470). The full width at half-maximum (fwhm) of the instrument response function (irf) was around 200 ps. Faster dynamics was investigated by fluorescence up-conversion (FU) using the same setup as in refs 31 and 32. Excitation was performed using 100 fs pulses produced by frequency doubling the output of a Ti:sapphire oscillator (Spectra-Physics, Mai Tai). The pump intensity on the sample was around 5 $\mu J/cm^2$, and the fwhm of the irf was ca. 200 fs. The sample solutions were located in a 0.4 mm rotating cell and had an absorbance of about 0.1 at the excitation wavelength.

Transient Absorption (TA) Spectroscopy. TA measurements were performed with two pump−probe setups. The femtosedond−picosecond TA setup used to record spectra up to 1.8 ns with an irf of ca. 150 fs (fwhm) has been described in detail elsewhere.[33,34] Excitation was performed using either 385 pulses generated by frequency doubling part of the output of a standard 1 kHz Ti:sapphire amplified system, or with pulses centered at 532 nm produced with a home-built noncollinear optical parametric amplifier. The intensity of the pump pulses on the sample was ca. 0.5 mJ/cm^2. The nanosecond−millisecond TA setup, used to record spectra up to 1 ms with an irf of 370 ps (fwhm), is the same as that described in refs 35 and 36. Excitation was performed either at 532 or at 355 nm using passively Q-switched, frequency doubled or tripled Nd:YAG lasers (Teem Photonics, Powerchip PNG-M02010, Powerchip NanoUV) producing pulses at 500 Hz repetition rate, with approximately 20 μJ energy per pulse, and 300 ps duration. The pump intensity on the sample was also around 0.5 mJ/cm^2. In both TA setups, probing was achieved using white light pulses generated by focusing 800 nm pulses in a CaF_2 plate and polarized at magic angle relative to the pump pulses. The sample solutions were located in a 1 mm quartz cell and were continuously stirred by N_2 bubbling. Their absorbance at the excitation wavelength was around 0.1. The solid samples were placed on a home-built two-dimension translation stage and were continuously translated in such a way to irradiate equally their entire surface area.

Quantum-Chemistry Calculations. Ground-state gas-phase geometry optimization of the triad was performed at the density functional level of theory (DFT) using the B3LYP functional and the 6-31G* basis set as implemented in Gaussian 09.[37]

RESULTS AND DISCUSSION

rNDI−pNDI−rNDI Triad. The electronic absorption spectrum of the triad in both DCM and ACN exhibits a broad band with a maximum at 534 nm originating from rNDI and due to a charge-transfer type $S_1 \leftarrow S_0$ transition involving the core substituents,[38] and a structured band below 400 nm that can be assigned to both the $S_2 \leftarrow S_0$ and the $S_1 \leftarrow S_0$ $\pi\pi^*$ transitions localized on rNDI and pNDI, respectively (Figure 2). Apart from a slight broadening on the red side of the $S_1 \leftarrow S_0$ band, the absorption spectrum of the trimer is almost identical to the sum of the pNDI and rNDI spectra with a 1:2 ratio, pointing to a relatively weak interaction between the chromophores.

DOI: 10.1021/acs.jpcc.5b04060
J. Phys. Chem. C 2015, 119, 14999−15008

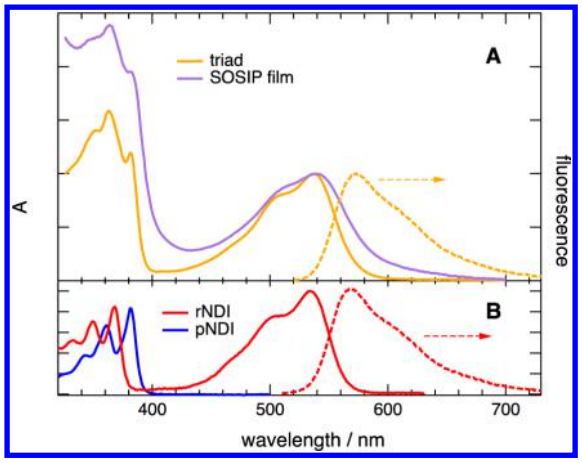

Figure 2. Absorption and fluorescence spectra of (A) the triad in DCM and of the SOSIP film and (B) rNDI and pNDI in DCM.

The fluorescence spectrum of the triad contains a single band centered around 570 nm that can be ascribed to the local $S_1 \rightarrow S_0$ rNDI transition.[28,38] The fluorescence excitation spectrum recorded at 570 nm exhibits both the $S_1 \leftarrow S_0$ and the $S_2 \leftarrow S_0$ bands of rNDI. However, the relative intensity of the $S_2 \leftarrow S_0$ band is approximately twice as small as in the absorption spectrum, pointing to an excitation-wavelength dependence of the fluorescence quantum yield. This effect has already been observed and investigated in detail with rNDI.[39] It is due to the presence of a $n\pi^*$ triplet state below the $\pi\pi^*$ S_2 state of rNDI and to the heavy Br substituent, which make intersystem crossing (ISC) from S_2 to the triplet manifold competitive with internal conversion to the S_1 state.

No triad emission originating from pNDI, known to fluoresce around 390 nm,[40,41] could be detected upon direct pNDI excitation. Additionally to the rNDI bands, the fluorescence excitation spectrum of the triad below 400 nm shows contribution from pNDI, in particular the distinct shoulder at 383 nm, which points to the occurrence of excitation energy transfer (EET) from the central pNDI to the peripheral rNDI units (Supporting Information Figure S1).

Whereas the fluorescence decay of rNDI measured by TCSPC was shown to be exponential with a lifetime around 5 ns,[39] that of the triad in both DCM and ACN required the sum of two exponential functions to be properly reproduced (Supporting Information Figure S2), with the time constants and average lifetimes listed in Table 1. Faster dynamics was measured at 570 and 620 nm by FU upon rNDI excitation. In ACN, about 30% of the initial intensity decays with a 5.5 ps time constant (Figure 3), unlike in DCM where no significant fast decay component was observed (Supporting Information Figure S3).

Table 1. Fluorescence Lifetimes, Relative Amplitudes (in Parentheses), and Average Lifetimes, τ_{av}

	τ_{fl1}	τ_{fl2}	τ_{fl3}	τ_{av}
rNDI/DCM	4.7 ns[a]			
rNDI/ACN	5.5 ns[a]			
triad/DCM	1.3 ns (0.20)	4.5 ns (0.80)		3.9 ns
triad/ACN	5.5 ps (0.29)	1.0 ns (0.13)	5.1 ns (0.58)	3.1 ns
SOSIP film	0.6 ps (0.38)	6.8 ps (0.41)	67 ps (0.31)	20 ps

[a]From ref 39.

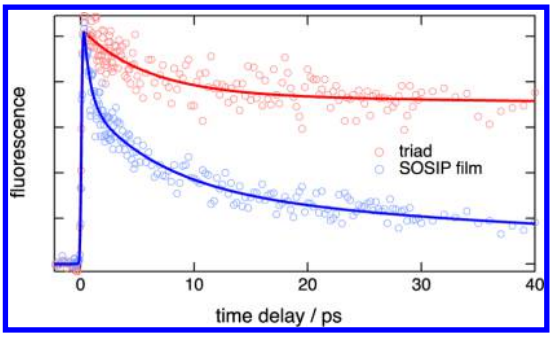

Figure 3. Early fluorescence dynamics at 570 nm measured with the triad in ACN and the SOSIP film upon rNDI excitation at 520 nm and best multiexponential fit.

The faster fluorescence dynamics of the trimer relatively to rNDI and its solvent polarity dependence point to a charge-transfer quenching process involving the nearby pNDI, which will be confirmed by the TA measurements. Because of its flexibility, the triad can adopt various conformations with different distances and mutual orientations of rNDI and pNDI. Although a thorough conformational analysis would require molecular dynamic simulations in solution, gas-phase geometry optimization of a hypothetical rNDI–pNDI dyad with different initial geometries indicates the existence of at least two different conformations of similar energy (Figure 4): (1) a folded one

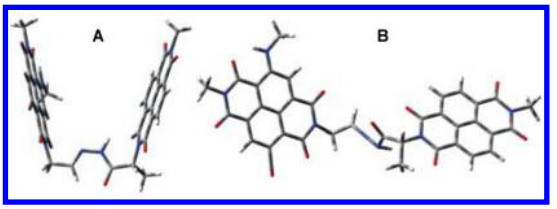

Figure 4. Gas-phase optimized folded (A) and unfolded (B) conformations of an rNDI–pNDI dimer.

with face-to-face chromophores and center-to-center distance of approximately 8 Å and (2) an unfolded conformation with center-to-center distance around 13 Å. As other conformations probably coexist in room-temperature solution phase, a broad distribution of quenching time constants and, thus, of fluorescence lifetimes can be expected.

More direct information on the EET from the pNDI to the rNDI unit was obtained from FU measurements of rNDI emission upon pNDI excitation at 385 nm. Although the signal-to-noise ratio of the data is substantially weaker than upon direct rNDI excitation, an initial rise of the fluorescence intensity with a 400 ± 100 fs time constant, that is, slower than the 200 fs irf, could be detected (Supporting Information Figure S3). Given the flexibility of the triad discussed above, slower EET components could also be expected. However, due to very efficient ISC, pNDI has a fluorescence lifetime of a few picoseconds only,[39,42] and, therefore, EET from pNDI has to be ultrafast to be competitive.

Further insight into the origin of the fluorescence quenching of the triad and its solvent dependence was obtained from TA measurements. The TA spectra recorded with the triad in DCM upon local rNDI excitation are essentially the same as those reported with rNDI alone (Figure 5A).[39] At early time, they are dominated by a positive band extending from 360 to 520 nm with maxima at 450 and 482 nm, which can be assigned

DOI: 10.1021/acs.jpcc.5b04060
J. Phys. Chem. C 2015, 119, 14999–15008

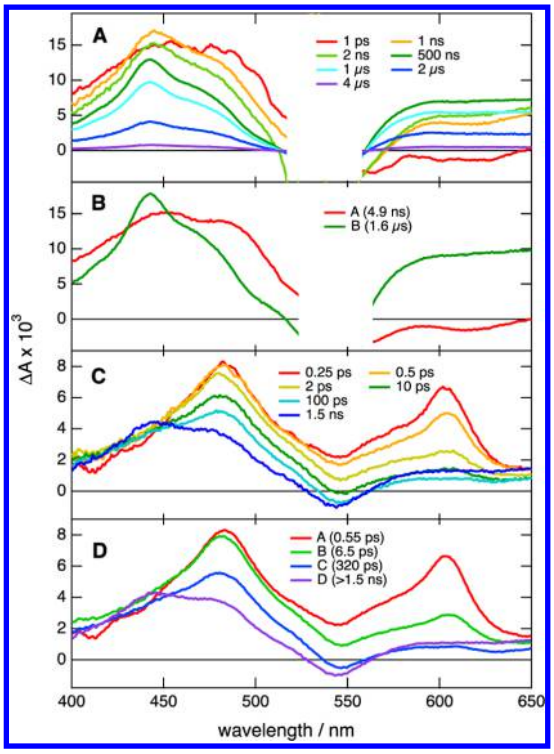

Figure 5. Transient absorption spectra measured with the triad in DCM upon (A) rNDI (532 nm), (C) pNDI (385 nm) excitation, and species-associated difference absorption spectra obtained from target analysis assuming sequential exponential steps (B,D).

to rNDI(S_1) absorption, and by two negative bands around 540 and 620 nm that are due to ground-state bleach and to $S_1 \rightarrow S_0$ stimulated emission, respectively. This spectrum evolves within a few nanoseconds into a spectrum that can be attributed to rNDI(T_1) characterized by two positive bands, the more intense peaking at 440 nm.[39] This spectrum remains unchanged, but its overall intensity decays to zero on a microsecond time scale. Although the fluorescence lifetime of the triad in DCM is slightly shorter than that of rNDI, no transient that could be ascribed to a quenching product can be identified. The TA data could be successfully reproduced by a global fit assuming a scheme with two consecutive exponential steps A → B → C,[43] where A and B are rNDI(S_1) and rNDI(T_1), with the time constants listed in Table 2 and the species-associated difference absorption spectra (SADS) shown in Figure 5B.

Table 2. Time Constants Obtained from the Transient Absorption Measurements

	excitation	τ_{TA1}	τ_{TA2}	τ_{TA3}	τ_{TA4}
triad in DCM	rNDI (532/355 nm)	4.9 ns	1.6 μs		
triad in DCM	pNDI (385 nm)	0.55 ps	6.5 ps	320 ps	>1.5 ns
triad in ACN	rNDI (532 nm)	4.1 ps	350 ps	1 μs	800 μs
triad in ACN	pNDI (385 nm)	0.2 ps	1.7 ps	90 ps	>1.5 ns
SOSIP film	rNDI (532 nm)	3.1 ps	31 ps	>1.5 ns	
SOSIP film	rNDI (355 nm)	2.3 ns	77 ns	2.2 μs	160 μs
SOSIP film	pNDI (385 nm)	0.2 ps	0.8 ps	16 ps	>1.5 ns

TA spectra up to 1.8 ns were also recorded upon local pNDI excitation of the triad at 385 nm. The spectra recorded within the first picosecond show the 605 nm absorption band of pNDI(S_1) (Figure 5C).[39,42] This band decays very rapidly, whereas a band at 480 nm rises and then decreases and shifts to shorter wavelengths on a subnanosecond time scale. Not less than four exponential functions were required to reproduce the TA dynamics; the SADS obtained assuming four successive steps are shown in Figure 5D. Whereas the first SADS originates mostly from pNDI(S_1), the second and third are very similar to each other and contain features that can be assigned to pNDI(T_1) (487 nm band)[39,42,44] and rNDI(S_1) (482 nm band and 625 nm dip). These steps can be attributed to $S_1 \rightarrow T_1$ ISC of pNDI as well as EET from pNDI(S_1) to rNDI(S_1). Finally, the last SADS can be assigned to rNDI(T_1). In principle, the latter can be populated by ISC from rNDI(S_1) and by triplet energy transfer from pNDI(T_1). The data do not allow establishing whether both or only one of these processes is operative. TA spectra were also recorded on a longer time scale upon 355 nm excitation. At this wavelength, about 2/3 of the absorption is due to rNDI, and the resulting transient spectra are very similar to those measured with rNDI alone upon $S_2 \leftarrow S_0$ excitation (Supporting Information Figure S4).[39]

Substantially more complicated dynamics were observed in ACN (Figure 6A). During the first nanosecond after rNDI excitation, the shape of the positive TA band between 400 and 500 nm changes: the maximum shifts from 460 to 475 nm during the first few picoseconds and then to 440 nm on a 300 ps time scale. During the same time, the negative band above 570 nm dominated by stimulated rNDI(S_1) emission trans-

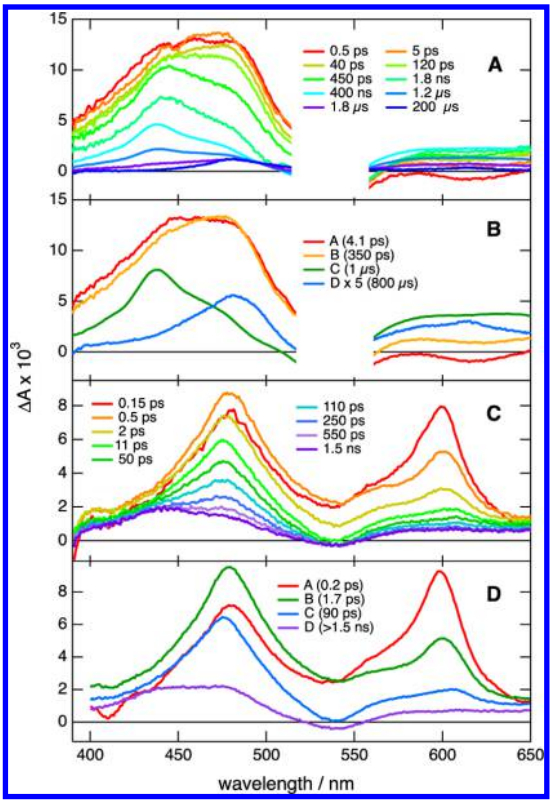

Figure 6. Transient absorption spectra measured with the triad in ACN upon (A) rNDI (532 nm), (C) pNDI (385 nm) excitation, and species-associated difference absorption spectra obtained from target analysis assuming sequential exponential steps (B,D).

DOI: 10.1021/acs.jpcc.5b04060
J. Phys. Chem. C 2015, 119, 14999−15008

forms into a positive band. After these fast changes, the TA spectrum evolves on a 1 μs time scale to a spectrum with two positive bands at ~482 and 610 nm, which has not fully decayed to zero after 1 ms. Four exponential functions were required to reproduce the TA dynamics, the SADS obtained assuming four successive steps being shown in Figure 6B. Whereas the first SADS can be assigned to rNDI(S_1), the second one most probably contains contributions from several intermediates. On the other hand, the third SADS is clearly dominated by rNDI(T_1). The fourth SADS strongly resembles the spectrum of the radical anion of a naphthalenediimide very similar to pNDI,[45] and can thus be assigned to a charge-separated (CS) state, with the electron on pNDI.

The TA dynamics can be explained in terms of the different triad conformations discussed above (Figure 7). Folded triads

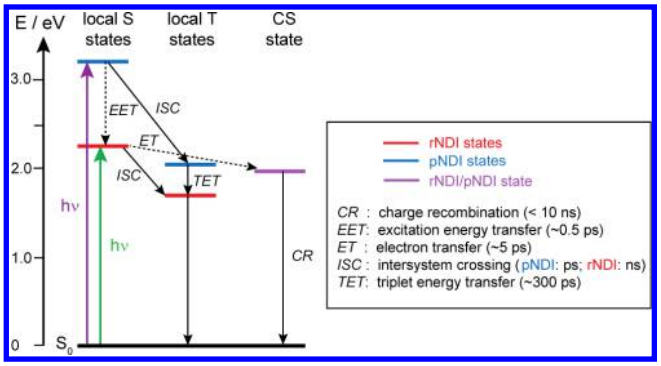

Figure 7. Energy level scheme of the trimer in ACN (in DCM, the CS state is about 0.5 eV higher) and most important processes with relevant time scales (bimolecular processes have been omitted). Dashed arrows: processes only operative in the folded conformation.

undergo fast electron transfer (ET) from the locally excited rNDI unit to pNDI. This process is not operative with the unfolded trimers, which decay by ISC to rNDI(T_1). Therefore, both rNDI(S_1) and the CS state contribute to the second SADS. Given the strong spectral overlap of the different intermediates, it is not possible to determine from these data whether the CS state population is only produced upon quenching of the folded triads or whether other conformations with larger rNDI–pNDI distances also undergo ET, but on a slower time scale.

Comparison of the SADS in DCM and ACN (Figures 5B and 6B) reveals that the relative population of rNDI(T_1) is about twice as small in ACN than in DCM. This difference can be accounted for by the occurrence of ET in ACN. If the entire CS state population were long-lived, a larger TA signal should be expected, especially considering the rather large absorption coefficient of $pNDI^{\bullet-}$.[45] Therefore, the small anion signal indicates that a large fraction of the CS state population undergoes faster charge recombination (CR). Because of the overlapping absorption bands of the various intermediates, the time scale of this CR cannot be determined. However, as the SADS assigned to rNDI(T_1) are very similar in ACN and DCM, contribution of the CS population is improbable. As a consequence, the CS state most probably only contributes to the second SADS, which decays with a 350 ps time constant.

The folding and unfolding of the triad, being mostly a diffusional process, can be expected to occur on a time scale shorter than the 0.8 ms lifetime of the long-lived CS state population. As a consequence, this long CS state lifetime cannot be explained by an unfolding of the triad after ET that would inhibit recombination. This $pNDI^{\bullet-}$ population most probably arises from a bimolecular process, triplet–triplet annihilation (TTA) between two triads with one of the two rNDIs in the T_1 state. Symmetry-breaking charge separation upon TTA has already been reported with several aromatic hydrocarbons and ketones in polar solvents.[46,47] TA measurements with rNDI revealed the formation of $rNDI^{\bullet-}$ upon TTA in ACN, but not in DCM.[39] This process should be operative with the triad as well. However, given the higher electron affinity of pNDI, the transferred electron, originally located on an rNDI, should rapidly hop to the pNDI, explaining the presence of $pNDI^{\bullet-}$ in the TA spectra. There is no spectral evidence for the presence of $rNDI^{\bullet+}$ that should also be produced during this process. However, previous investigations on an analogue of rNDI with a Cl instead of a Br substituent indicated that the radical cation has either an absorption spectrum very similar to that of the anion or a weak absorption in the visible region.[48]

Significant differences can be observed at early time delays after local pNDI excitation in ACN (Figure 6C). The initial TA spectra consist of the pNDI(S_1) band at 605 nm, which decays very rapidly, whereas a band appears at 480 nm. Afterward, this 480 nm band shows a first partial decay and shift to 475 nm, and then another decay, a further shift, and a broadening. Additionally, a negative band around 540 nm that can be assigned to the bleach of rNDI appears after a few picoseconds and remains present up to 1.8 ns, the upper limit of the time window. Target analysis assuming four successive exponential steps could reproduce the TA data, with the time constants listed in Table 2 and the SADS shown in Figure 6D. Whereas the first of them can be safely assigned to pNDI(S_1), the second and third SADS should contain contributions from pNDI(T_1) populated upon ISC, rNDI(S_1) populated upon EET, and possibly the CS state. Finally, the last SADS shows features that can be assigned to rNDI(T_1) and to the CS state. Given the large number of intermediates and their overlapping spectra, a quantitative interpretation of this TA dynamics is not possible. However, the data suggest that rapid EET from pNDI(S_1) to rNDI(S_1), followed by charge separation, occurs in the folded triads.

SOSIP Architecture. The electronic absorption spectrum of the surface architecture is similar to that of the triad in solution, but the band in the visible region exhibits a broadening that can be attributed to the excitonic coupling between the π-stacked rNDIs (Figure 1). The higher relative intensity of the short wavelength absorption band in the SOSIP film can be explained by the scattering caused by the film and/or by hypochromism of the rNDI $S_1 \leftarrow S_0$ band.

No distinct stationary emission spectrum could be detected with the film, pointing to a negligibly small fluorescence quantum yield. This is consistent with the very short fluorescence lifetime revealed by FU measurements (Figure 3). The fluorescence dynamics at 570 and 600 nm measured upon rNDI excitation required the sum of three exponential functions, with an average decay time around 20 ps, to be properly reproduced (Table 1). This indicates that the negligible fluorescence of the SOSIP film is not, at least not entirely, due to the formation of nonemissive aggregates in the rNDI stacks. Very similar dynamics was observed upon pNDI excitation at 385 nm. Because of the small signal-to-noise ratio, only an approximate fluorescence rise time of ~200 fs could be estimated (Supporting Information Figure S5). Nevertheless,

DOI: 10.1021/acs.jpcc.5b04060
J. Phys. Chem. C 2015, 119, 14999–15008

this result reveals that EET from pNDI(S_1) to rNDI is also operative in the surface architecture.

TA measurements up to 1.8 ns were carried out upon both local rNDI and pNDI excitation, at 530 and 385 nm, respectively (Figures 8). Measurements on a longer time

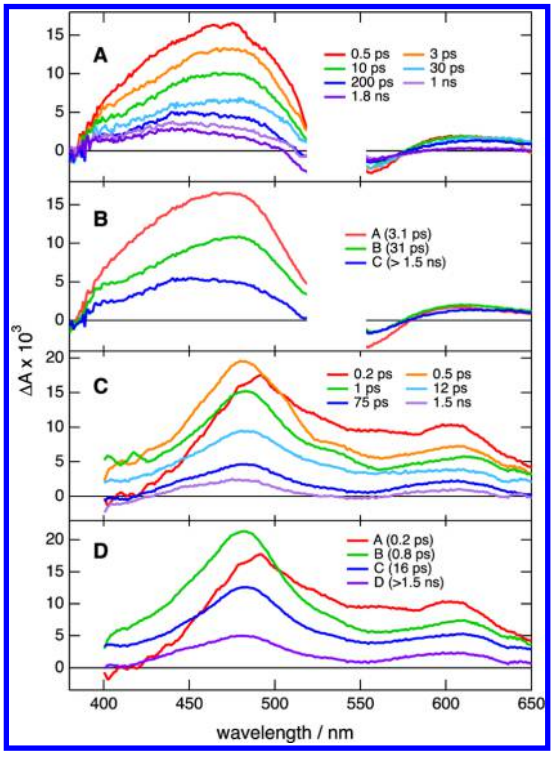

Figure 8. Transient absorption spectra measured with the SOSIP film upon (A) rNDI (532 nm), (C) pNDI (385 nm) excitation, and species-associated difference absorption spectra obtained from target analysis assuming sequential exponential steps (B,D).

scale were also performed upon 355 nm (mostly rNDI $S_2 \leftarrow S_0$) excitation (Figure 9). The main feature in the TA spectra upon 532 nm excitation is the broad positive band in the 400–500 nm region, whose shape changes and intensity decreases by

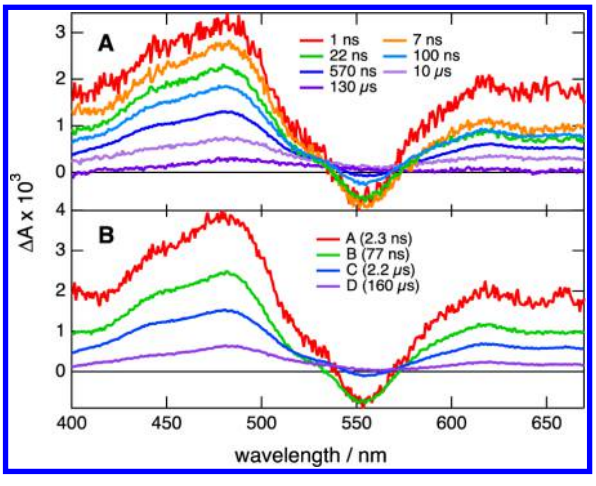

Figure 9. Transient absorption spectra measured with the SOSIP film upon 355 nm excitation (A) and species-associated difference absorption spectra obtained from target analysis assuming sequential exponential steps (B).

a factor of more than 3 within the experimental time window (Figure 8A). The SADS obtained from a global analysis do not exhibit very pronounced differences (Figure 8B). From a comparison with the SADS obtained with the triad alone (Figure 6), and in view of the FU measurements (Figure 3), one can safely assign the first SADS to rNDI(S_1), or to an exciton localized in a rNDI stack. The second SADS is similar but not identical to the first and, according to the FU measurements, should contain a contribution from rNDI(S_1). The more pronounced intensity at 480 nm could be due to $pNDI^{\bullet-}$. Finally, the band in the third SADS shows a maximum at 445 nm, which could be attributed to rNDI(T_1), together with a shoulder at 480 nm possibly originating from $pNDI^{\bullet-}$.

The TA spectra recorded upon pNDI excitation show even less spectral evolution (Figure 8C). The earliest spectra contain features from pNDI(S_1), and very quickly transform into a spectrum with a band in the 400–500 nm region that is narrower than that found upon rNDI excitation. At later time delays, the shape of the spectrum remains mostly unchanged but the intensity decays on multiple time scales. Global analysis required four exponential functions, one for the initial decay pNDI(S_1) and three for following dynamics. The SADS related to the multiphasic decay are essentially identical and very similar to the spectrum of $pNDI^{\bullet-}$ (Figure 8D). They can thus be ascribed to a CS state, although other intermediates, such as rNDI(S_1), should also contribute at early time.

The early TA spectra measured with 355 nm pump pulses resemble those measured at similar time delays upon 532 nm excitation, confirming that absorption at this wavelength is mostly due to rNDI. They consist of a band peaking at 480 nm with a shoulder at 440 nm, a negative band around 550 nm, and a positive one centered around 610 nm (Figure 9). The spectra do not change much with time, and the decay can be reproduced with a sum of four exponential functions (Table 2). In this case again, the 480 and 610 nm band can be assigned to $pNDI^{\bullet-}$, whereas the 440 nm band is most probably due to rNDI(T_1).

This ensemble of data indicates that the charge-transfer dynamics in the SOSIP architecture depends on whether rNDI or pNDI is initially excited. After direct excitation of an rNDI, a CS state, with the electron on pNDI, as well as rNDI(T_1) are populated. On the other hand, excitation of pNDI is followed by the population of the CS state in parallel with EET to rNDI(S_1), which itself decays as discussed just above. Overall, charge separation is more efficient upon pNDI than rNDI excitation. The TA data do not exhibit any feature that could hint at the location of the hole. Considering the redox properties of the constituents, the energetically most stable CS state should be that with the hole on an rNDI, as in the triad.

Comparison between the Triad in Solution and the SOSIP Film. The results reveal that charge separation in the SOSIP film is much more efficient than that in the triad. In the latter case, significant ET from an excited rNDI to pNDI is only observed in ACN and with a subpopulation of trimers with a proper conformation. The donor–acceptor distance in the unfolded triads is probably too large to ensure ET within the 5 ns lifetime of rNDI(S_1).

In principle, the rNDI–pNDI distance in the surface architecture should be similar to that in the unfolded triad and should not favor ultrafast charge separation. However, π stacking and close lateral proximity of the π stacks in the SOSIP film result in short distances between identical NDIs that open charge-transfer pathways that are not operative in the isolated

DOI: 10.1021/acs.jpcc.5b04060
J. Phys. Chem. C 2015, 119, 14999–15008

triad. For example, symmetry-breaking charge separation between an rNDI in the S_1 state and an rNDI in the ground state is energetically favorable but cannot occur in the triad because these two units are too far apart. However, such process is feasible in the SOSIP film, and, according to the redox potentials of rNDI,[28] this symmetry-broken CS state should be located about 0.1 eV above the rNDI/pNDI CS state (Figure 10). The energy difference might be even smaller if

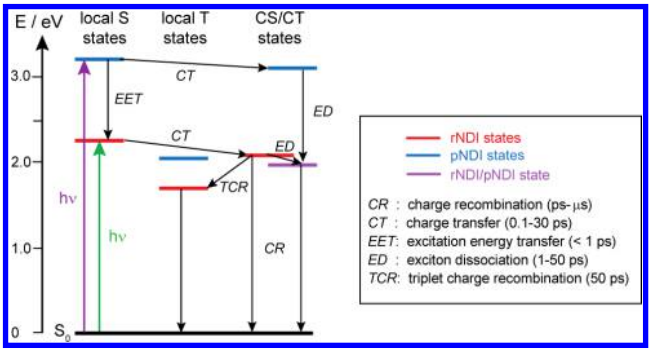

Figure 10. Energy level scheme pertaining to the SOSIP film and most important processes with relevant time scales.

electrostatic interaction is taken into account. Therefore, rNDI excitation of the SOSIP results in a Frenkel-type exciton that should be mostly localized on a single rNDI, and that rapidly transforms into a CT-exciton localized on two rNDIs. As the excited states and radical ions of rNDI and pNDI absorb in the 400−500 nm region, there is no unambiguous experimental evidence of this CT-exciton. However, considering that $rNDI^{\bullet-}$ absorbs around 450 nm,[39] the CT-exciton could be responsible for the broadening of the 400−450 nm band observed at short time delays.

The TA data show that both the rNDI/pNDI CS state and $rNDI(T_1)$ are rapidly populated. This most probably occurs through the parallel dissociation and recombination of the CT-exciton, respectively. Given the very fast decay of the fluorescence, population of $rNDI(T_1)$ by ISC from the S_1 state should be very inefficient. However, as $rNDI(T_1)$ is located below the CT-excitonic state, and because of the bromine atom, triplet recombination should be efficient, as previously observed for the recombination of geminate ions pairs containing heavy atoms.[49]

From the bleach of the rNDI absorption around 550 nm, the overall exciton dissociation and triplet recombination efficiency can be approximately estimated to be around 0.5. The assumption that the absorption coefficient of $rNDI(T_1)$ is similar to that of $pNDI(T_1)$ yields a charge-separation efficiency of the order of 0.15. This relatively modest value is probably caused by the rigid and weakly polar environment in the SOSIP film that slows the dissociation of the CT-exciton and favors recombination to either the triplet or the ground state. As the so-generated triplet excitons diffuse in the rNDI stack, two of them can encounter and form again a CT-exciton upon annihilation, as observed at long time delay with the triad in ACN.

On the other hand, pNDI excitation of the SOSIP results in the population of a Frenkel-type exciton localized on a pNDI. The corresponding TA spectrum transforms in less than 1 ps to another dominated by $pNDI^{\bullet-}$. However, the location of the hole is not clear. TA measurements with pNDI alone indicate that, as for rNDI, symmetry-breaking charge separation upon TTA is operative in ACN but not in DCM.[39] Although the oxidation potential of pNDI is not known, the energy of the pNDI CT-excitonic state can be expected to be well above the rNDI/pNDI CS state. Therefore, the driving force for dissociation into this CS state should be sufficiently large to make this process very fast.

The absence of the ground-state bleach feature in the TA spectra does not allow the charge-separation efficiency to be deduced. However, the TA signal associated with this CS state loses about 2/3 of its amplitude within 20−30 ps, pointing to the existence of fast recombination processes.

The TA data recorded up to 1 ms reveal that CR occurs on a wide range of time scales, that is, from a few picoseconds to hundreds of microseconds. The faster components are most probably due to geminate recombination, that is, recombination occurring before the diffusion of the charges in their respective π stacks. Although the rNDI−pNDI distance is larger than within the stacks, some Coulombic attraction might still slow the dissociation of this weakly bound exciton into free charge carriers. Close lateral proximity of neighboring π-stacks and eventual structural defects could afford short rNDI−pNDI distances and thus facilitate CR.

The longer-lived $pNDI^{\bullet-}$ components indicate that the charges diffuse apart in the rNDI and pNDI stacks, which act as p and n conductors, respectively.[50] As the surface architecture is not integrated into an electric circuit, these free charges are not extracted and, thus, eventually recombine. Although the observed recombination dynamics seems to be well accounted for by a sum of exponential functions, Figure 11 shows that the

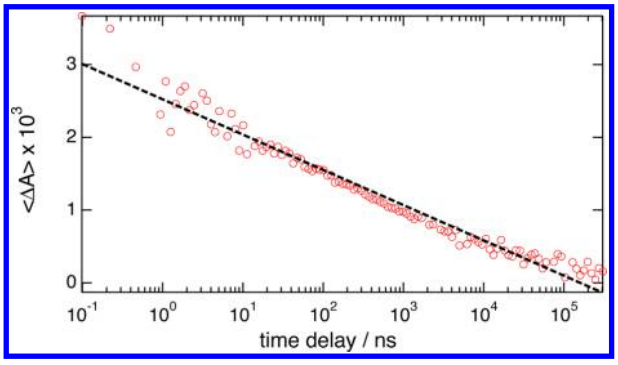

Figure 11. Logarithmic time-dependence of the average TA signal between 470 and 500 nm due to $pNDI^{\bullet-}$, measured with the SOSIP film upon 355 nm excitation and best linear fit (dashed line).

decay of $pNDI^{\bullet-}$ population almost follows a logarithmic time dependence. Such temporal behavior has already been reported for various phenomena, such as energy relaxation in Coulomb glasses,[51] phase transformation in high pressure glasses,[52] tunneling processes in low temperature polymers,[53,54] exchange kinetics of copolymer matrices,[55] DNA internal dynamics,[56] or protein folding.[57] This dependence has been explained by a very broad distribution of activation energies, or an exponential distribution of local minima. The close to logarithmic time dependence found here for the CR in the film might be coincidental and would need further measurements at different excitation intensities to be confirmed. In any cases, the CR dynamics of the surface architecture differs from that reported so far with polymer-based bulk heterojunctions,[58−63] and exhibits substantially slower components. This difference might arise from the supramolecular organization of the SOSIP film that should favor charge separation and conduction and from

DOI: 10.1021/acs.jpcc.5b04060
J. Phys. Chem. C 2015, 119, 14999−15008

the delayed formation of CT-exciton by triplet−triplet annihilation.

CONCLUDING REMARKS

This investigation reveals that the initial photoinduced charge separation pathway in the SOSIP architecture differs from that in the model triad in solution. Although the results obtained with the trimer are useful as they allow a relevant charge separation process to be identified, they are clearly not sufficient to account for the generation of a photocurrent in the surface architecture. In the triad, the number of interactions of the excited chromophore is limited to those with the two other constituting units. Given the small concentration of triad, bimolecular "intertriad" interactions are not operative during the singlet excited-state lifetime, but they can take place within the lifetime of the triplet excited state.

In the SOSIP film, "intertriad" interactions are strongly enhanced and result in rapid photoinduced symmetry-breaking charge separation. This process plays a key role as it leads to the ultrafast population of a charge transfer excitonic state, which can migrate along a π stack and eventually dissociates into a state with both charges located in separated stacks, where Coulombic attraction is much smaller and where the charges can more easily diffuse apart.

A SOSIP architecture based on chromophores that, contrary to those used here, do not undergo symmetry-breaking charge separation could be expected to exhibit weaker photoconductivity, as the latter would require the direct dissociation of a Frenkel type exciton to loosely bound CT-exciton. Although symmetry-breaking charge separation has, until now, been demonstrated with a limited number of molecules, among them several core-substituted NDIs, it should be rather common and is worth being exploited when designing multichromophoric photoactive systems.

The time scale of charge recombination upon laser pulse excitation of the SOSIP film spans 7−8 orders of magnitude. Different dynamics, especially slower nongeminate recombination, can be anticipated under solar illumination and in the presence of a bias voltage. Further slowing of recombination could be expected with a triple-channel SOSIP architecture, that is, by separating the n and p channels by an insulating channel. This could be done by replacing one of the rNDIs by a unit with better electron-accepting properties than pNDI or by introducing matching dyads rather than rNDI monomers only by stack exchange. The latter, more practical approach to triple-channel photosystems has been explored recently for several combinations of chromophores.[64−66]

ASSOCIATED CONTENT

Supporting Information

Synthesis of the trimer, fluorescence excitation spectra, time-correlated single photon counting and fluorescence up conversion data, and transient absorption spectra. The Supporting Information is available free of charge on the ACS Publications website at DOI: 10.1021/acs.jpcc.5b04060.

AUTHOR INFORMATION

Corresponding Authors

*E-mail: stefan.matile@unige.ch.
*E-mail: eric.vauthey@unige.ch.

Notes

The authors declare no competing financial interest.

ACKNOWLEDGMENTS

This work was supported by the Swiss National Science Foundation through project nos. 200020-147098 and 200020-150000, and the University of Geneva, the European Research Council (ERC Advanced Investigator), the National Centre of Competence in Research (NCCR) Chemical Biology, and the NCCR Molecular Systems Engineering.

REFERENCES

(1) Holten, D.; Bocian, D. F.; Lindsey, J. S. Probing Electronic Communication in Covalently Linked Multiporphyrin Arrays. A Guide to the Rational Design of Molecular Photonics Devices. *Acc. Chem. Res.* **2002**, *35*, 57−69.
(2) Imahori, H. Giant Multiporphyrin Arrays as Artificial Light-Harvesting Antennas. *J. Phys. Chem. B* **2004**, *108*, 6130−6143.
(3) Bhosale, S.; L, S. A.; Talukdar, P.; Fürstenberg, A.; Banerji, N.; Vauthey, E.; Bollot, G.; Mareda, J.; Röger, C.; Würthner, F.; et al. Photoproduction of Proton Gradients with Pi-Stacked Fluorophore Scaffolds in Lipid Bilayers. *Science* **2006**, *313*, 84−86.
(4) Sakai, N.; Sisson, A. L.; Bürgi, T.; Matile, S. Zipper Assembly of Photoactive Rigid-Rod Naphthalenediimide -Stack Architectures on Gold Nanoparticles and Gold Electrode. *J. Am. Chem. Soc.* **2007**, *129*, 15758−15759.
(5) Wasielewski, M. R. M. Self-Assembly Strategies for Integrating Light Harvesting and Charge Separation in Artificial Photosynthetic Systems. *Acc. Chem. Res.* **2009**, *42*, 1910−21.
(6) Bottari, G.; de la Torre, G.; Guldi, D. M.; Torres, T. Covalent and Noncovalent Phthalocyanine−Carbon Nanostructure Systems: Synthesis, Photoinduced Electron Transfer, and Application to Molecular Photovoltaics. *Chem. Rev.* **2010**, *110*, 6768−6816.
(7) Würthner, F.; Meerholz, K. Systems Chemistry Approach in Organic Photovoltaics. *Chem.—Eur. J.* **2010**, *16*, 9366−9373.
(8) Astruc, D.; Boisselier, E.; Ornelas, C. Dendrimers Designed for Functions: From Physical, Photophysical, and Supramolecular Properties to Applications in Sensing, Catalysis, Molecular Electronics, Photonics, and Nanomedicine. *Chem. Rev.* **2010**, *110*, 1857−1959.
(9) Pellegrin, Y.; Odobel, F. Molecular Devices Featuring Sequential Photoinduced Charge Separations for the Storage of Multiple Redox Equivalents. *Coord. Chem. Rev.* **2011**, *255*, 2578−2593.
(10) Sakai, N.; Lista, M.; Kel, O.; Sakurai, S.-i.; Emery, D.; Mareda, J.; Vauthey, E.; Matile, S. Self-Organizing Surface-Initiated Polymerization: Facile Access to Complex Functional Systems. *J. Am. Chem. Soc.* **2011**, *133*, 15224−15227.
(11) Charvet, R.; Yamamoto, Y.; Sasaki, T.; Kim, J.; Kato, K.; Takata, M.; Saeki, A.; Seki, S.; Aida, T. Segregated and Alternately Stacked Donor/Acceptor Nanodomains in Tubular Morphology Tailored with Zinc Porphyrin−C60 Amphiphilic Dyads: Clear Geometrical Effects on Photoconduction. *J. Am. Chem. Soc.* **2012**, *134*, 2524−2527.
(12) Sundström, V. Femtobiology. *Annu. Rev. Phys. Chem.* **2008**, *59*, 53−77.
(13) van Grondelle, R.; Novoderezhkin, V. I. Photosynthesis: Quantum Design for a Light Trap. *Nature* **2010**, *463*, 614−615.
(14) Hohmann-Marriott, M. F.; Blankenship, R. E. Evolution of Photosynthesis. *Annu. Rev. Plant Biol.* **2011**, *62*, 515−548.
(15) Osswald, P.; You, C.-C.; Stepanenko, V.; Würthner, F. DABCO-Mediated Self-Assembly of Zinc Porphyrin−Perylene Bisimide Monodisperse Multichromophoric Nanoparticles. *Chem.—Eur. J.* **2010**, *16*, 2386−2390.
(16) Röger, C.; Müller, M. G.; Lysetska, M.; Miloslavina, Y.; Holzwarth, A. R.; Würthner, F. Efficient Energy Transfer from Peripheral Chromophores to the Self-Assembled Zinc Chlorin Rod Antenna: A Bioinspired Light-Harvesting System to Bridge the "Green Gap". *J. Am. Chem. Soc.* **2006**, *128*, 6542−6543.
(17) Kasha, M.; Rawls, H. R.; El-Bayoumi, M. A. The Exciton Model in Molecular Spectroscopy. *Pure Appl. Chem.* **1965**, *11*, 371−392.
(18) van Amerongen, H.; Valkunas, L.; van Grondelle, R. *Photosynthetic Excitons*; World Scientific: Singapore, 2000.

DOI: 10.1021/acs.jpcc.5b04060
J. Phys. Chem. C 2015, 119, 14999−15008

(19) Jenkins, R. D.; Andrews, D. L. Multichromophore Excitons and Resonance Energy Transfer: Molecular Quantum Electrodynamics. *J. Chem. Phys.* **2003**, *118*, 3470.
(20) Spano, F. C.; Silva, C. H- and J-Aggregate Behavior in Polymeric Semiconductors. *Annu. Rev. Phys. Chem.* **2014**, *65*, 477−500.
(21) Hattori, S.; Ohkubo, K.; Urano, Y.; Sunahara, H.; Nagano, T.; Wada, Y.; Tkachenko, N. V.; Lemmetyinen, H.; Fukuzumi, S. Charge Separation in a Nonfluorescent Donor-Acceptor Dyad Derived from Boron Dipyrromethene Dye, Leading to Photocurrent Generation. *J. Phys. Chem. B* **2005**, *109*, 15368−15375.
(22) Kodis, G.; Terazono, Y.; Liddell, P. A.; Andréasson, J.; Garg, V.; Hambourger, M.; Moore, T. A.; Moore, A. L.; Gust, D. Energy and Photoinduced Electron Transfer in a Wheel-Shaped Artificial Photosynthetic Antenna-Reaction Center Complex. *J. Am. Chem. Soc.* **2006**, *128*, 1818−1827.
(23) Chaignon, F.; Falkenstrom, M.; Karlsson, S.; Blart, E.; Odobel, F.; Hammarström, L. Very Large Acceleration of the Photoinduced Electron Transfer in a Ru(bpy)3-Naphthalene Bisimide Dyad Bridged on the Naphthyl Core. *Chem. Commun.* **2007**, 64−66.
(24) Dance, Z. E. X.; Ahrens, M. J.; Vega, A. M.; Ricks, A. B.; McCamant, D. W.; Ratner, M. A.; Wasielewski, M. R. Direct Observation of the Preference of Hole Transfer over Electron Transfer for Radical Ion Pair Recombination in Donor-Bridge-Acceptor Molecules. *J. Am. Chem. Soc.* **2008**, *130*, 830−832.
(25) Lembo, A.; Tagliatesta, P.; Guldi, D. M.; Wielopolski, M.; Nuccetelli, M. Porphyrin/Oligo-Ethynylenephenylene/Fullerene Triads: Synthesis and Electrochemical and Photophysical Characterization of the New Porphyrin-Oligo-PPE-Fullerene Systems. *J. Phys. Chem. A* **2009**, *113*, 1779−1793.
(26) Villamaina, D.; Bhosale, S.; Langford, S. J.; Vauthey, E. Excited-State Dynamics of Porphyrin-Naphthalenediimide-Porphyrin Triads. *Phys. Chem. Chem. Phys.* **2013**, *15*, 1177−1187.
(27) Sakai, N.; Matile, S. Stack Exchange Strategies for the Synthesis of Covalent Double-Channel Photosystems by Self-Organizing Surface-Initiated Polymerization. *J. Am. Chem. Soc.* **2011**, *133*, 18542−18545.
(28) Sakai, N.; Mareda, J.; Vauthey, E.; Matile, S. Core-Substituted Naphthalenediimides. *Chem. Commun.* **2010**, *46*, 4225−4237.
(29) Muller, P.-A.; Högemann, C.; Allonas, X.; Jacques, P.; Vauthey, E. Deuterium Isotope Effect on the Charge Recombination Dynamics of Contact Ion Pairs Formed by Electron Transfer Quenching in Acetonitrile. *Chem. Phys. Lett.* **2000**, *326*, 321−327.
(30) Fürstenberg, A.; Vauthey, E. Excited State Dynamics of the Fluorescent Probe Lucifer Yellow in Liquid Solutions in in Heterogeneous Media. *Photochem. Photobiol. Sci.* **2005**, *4*, 260−267.
(31) Morandeira, A.; Engeli, L.; Vauthey, E. Ultrafast Charge Recombination of Photogenerated Ion Pairs to an Electronic Excited State. *J. Phys. Chem. A* **2002**, *106*, 4833−4837.
(32) Duvanel, G.; Grilj, J.; Chaumeil, H.; Jacques, P.; Vauthey, E. Ultrafast Excited-State Dynamics of a Series of Zwitterionic Pyridinium Phenoxides with Increasing Sterical Hindering. *Photochem. Photobiol. Sci.* **2010**, *9*, 908−915.
(33) Duvanel, G.; Banerji, N.; Vauthey, E. Excited-State Dynamics of Donor-Acceptor Bridged Systems Containing a Boron-Dipyrromethene Chromophore: Interplay between Charge Separation and Reorientational Motion. *J. Phys. Chem. A* **2007**, *111*, 5361−5369.
(34) Banerji, N.; Duvanel, G.; Perez-Velasco, A.; Maity, S.; Sakai, N.; Matile, S.; Vauthey, E. Excited-State Dynamics of Hybrid Multichromophoric Systems: Toward an Excitation Wavelength Control of the Charge Separation Pathways. *J. Phys. Chem. A* **2009**, *113*, 8202−8212.
(35) Lang, B.; Mosquera-Vazquez, S.; Lovy, D.; Sherin, P.; Markovic, V.; Vauthey, E. Broadband Ultraviolet-Visible Transient Absorption Spectroscopy in the Nanosecond to Microsecond Time Domain with Sub-Nanosecond Time Resolution. *Rev. Sci. Instrum.* **2013**, *84*, 073107−8.
(36) Yushchenko, O.; Hangarge, R. V.; Mosquera-Vazquez, S.; Bhosale, S. V.; Vauthey, E. Electron, Hole, Singlet and Triplet Energy Transfer in Photoexcited Porphyrin-naphthalenediimide Dyads. *J. Phys. Chem. B* **2015**, *119*.
(37) Frisch, M. J.; Trucks, G. W.; Schlegel, H. B.; Scuseria, G. E.; Robb, M. A.; Cheeseman, J. R.; Scalmani, G.; Barone, V.; Mennucci, B.; Petersson, G. A.; et al. *Gaussian 09*, revision C1; Gaussian, Inc.: Wallingford, CT, 2010.
(38) Würthner, F.; Shahadat, A.; Thalacker, C.; Debaerdemaeker, T. Core-Substituted Naphthalene Bisimides: New Fluorophors with Tunable Emission Wavelength for FRET Studies. *Chem.—Eur. J.* **2002**, *8*, 4742.
(39) Yushchenko, O.; Licari, G.; Mosquera-Vazquez, S.; Sakai, N.; Matile, S.; Vauthey, E. Ultrafast Intersystem-Crossing Dynamics and Breakdown of the Kasha−Vavilov's Rule of Naphthalenediimides. *J. Phys. Chem. Lett.* **2015**, *6*, 2096−2100.
(40) Barros, T. C.; Brochsztain, S.; Toscano, V. G.; Berci Filho, P.; Politi, M. J. Photophysical characterization of a 1,4,5,8-naphthalenediimide derivative. *J. Photochem. Photobiol., A* **1997**, *111*, 97−104.
(41) Alp, S.; Erten, S.; Karapire, C.; Koz, B.; Doroshenko, A. O.; Icli, S. Photoinduced Energy-Electron Transfer Studies with Naphthalene Diimides. *J. Photochem. Photobiol., A* **2000**, *135*, 103−110.
(42) Ganesan, P.; Baggerman, J.; Zhang, H.; Sudholter, E. J. R.; Zuilhof, H. Femtosecond Time-Resolved Photophysics of 1,4,5,8-Naphthalene Diimides. *J. Phys. Chem. A* **2007**, *111*, 6151−6156.
(43) van Stokkum, I. H. M.; Larsen, D. S.; van Grondelle, R. Global and Target Analysis of Time-Resolved Spectra. *Biochim. Biophys. Acta, Bioenerg.* **2004**, *1657*, 82−104.
(44) Abraham, B.; McMasters, S.; Mullan, M. A.; Kelly, L. A. Reactivities of Carboxyalkyl-Substituted 1,4,5,8-Naphthalene Diimides in Aqueous Solution. *J. Am. Chem. Soc.* **2004**, *126*, 4293−4300.
(45) Gosztola, D.; Niemczik, M. P.; Svec, W.; Lukas, A. S.; Wasielewski, M. R. Excited Doublet States of Electrochemically Generated Aromatic Imide and Diimide Radical Anions. *J. Phys. Chem. A* **2000**, *104*, 6545−6551.
(46) Jarnagin, R. C. Photoionization Processes in Organic Solids and Fluids. *Acc. Chem. Res.* **1971**, *4*, 420−7.
(47) Jacques, P.; Allonas, X.; Sarbach, A.; Haselbach, E.; Vauthey, E. Tuning the Ion Formation Processes from Triplet-Triplet Annihilation to Triplet Mediated Photoionisation. *Chem. Phys. Lett.* **2003**, *378*, 185.
(48) Banerji, N.; Fürstenberg, A.; Bhosale, S.; Sisson, A. L.; Sakai, N.; Matile, S.; Vauthey, E. Ultrafast Photoinduced Charge Separation in Naphthalene Diimide Based Multichromophoric Systems in Liquid Solutions and in a Lipid Membrane. *J. Phys. Chem. B* **2008**, *112*, 8912−8922.
(49) Nicolet, O.; Vauthey, E. Heavy Atom Effect on the Charge Recombination Dynamics of Photogenerated Geminate Ion Pairs. *J. Phys. Chem. A* **2003**, *107*, 5894−5902.
(50) Bhosale, R.; Misek, J.; Sakai, N.; Matile, S. Supramolecular n/p-Heterojunction Photosystems withOriented Multicolored Antiparallel Redox Gradients (OMARG-SHJs). *Chem. Soc. Rev.* **2010**, *39*, 138−149.
(51) Glatz, A.; Vinikur, V. M.; Galperin, Y. M. Statistics of Deep Energy Stated in Coulomb Glasses. *Phys. Rev. Lett.* **2007**, *98*, 196401.
(52) Tsiok, O. B.; Brazhkin, V. V.; Lyapin, A. G.; Khvostantsev, L. G. Logarithmic Kinetics of the Amorphous-Amorphous Transformations in SiO2 and GeO2 Glasses under High Pressure. *Phys. Rev. Lett.* **1998**, *80*, 999−1002.
(53) Breinl, W.; Friedrich, J.; Haarer, D. Logarithmic Decay of Photochemically Induced Two-Level Systems in an Organic Glass. *Chem. Phys. Lett.* **1984**, *106*, 487.
(54) Vauthey, E.; Voss, J.; Caro, C. D.; Renn, A.; Wild, U. P. Spectral Hole Burning Study of Squaraine Dyes in Polymer Films. *J. Lumin.* **1993**, *56*, 61−69.
(55) Lund, R.; Willner, L.; Richter, D.; Dormidontova, E. E. Equilibrium Chain Exchange Kinetics of Diblock Copolymer Micelles: Tuning and Logarithmic Relaxation. *Macromolecules* **2006**, *39*, 4566−4575.
(56) Brauns, E. B.; Madaras, M. L.; Coleman, R. S.; Murphy, C. J.; Berg, M. A. Complex Local Dynamics in DNA on the Picosecond and Nanosecond Time Scales. *Phys. Rev. Lett.* **2002**, *88*, 158101.

DOI: 10.1021/acs.jpcc.5b04060
J. Phys. Chem. C 2015, 119, 14999−15008

(57) Skorobogatiy, M.; Guo, H.; Zuckermann, M. Non-Arrhenius Modes in the Relaxation of Model Proteins. *J. Chem. Phys.* **1998**, *109*, 2528−2535.
(58) Pal, S. K.; Kesti, T.; Maiti, M.; Zhang, F.; Inganäs, O.; Hellström, S.; Andersson, M. R.; Oswald, F.; Langa, F.; Österman, T.; et al. Geminate Charge Recombination in Polymer/Fullerene Bulk Heterojunction Films and Implications for Solar Cell Function. *J. Am. Chem. Soc.* **2010**, *132*, 12440−12451.
(59) Dimitrov, S. D.; Bakulin, A. A.; Nielsen, C. B.; Schroeder, B. C.; Du, J.; Bronstein, H.; McCulloch, I.; Friend, R. H.; Durrant, J. R. On the Energetic Dependence of Charge Separation in Low-Band-Gap Polymer/Fullerene Blends. *J. Am. Chem. Soc.* **2012**, *134*, 18189−18192.
(60) Credgington, D.; Jamieson, F. C.; Walker, B.; Nguyen, T.-Q.; Durrant, J. R. Quantification of Geminate and Non-Geminate Recombination Losses within a Solution-Processed Small-Molecule Bulk Heterojunction Solar Cell. *Adv. Mater.* **2012**, *24*, 2135−2141.
(61) Heeger, A. J. 25th Anniversary Article: Bulk Heterojunction Solar Cells: Understanding the Mechanism of Operation. *Adv. Mater.* **2014**, *26*, 10−28.
(62) Günes, S.; Neugebauer, H.; Sariciftci, N. S. Conjugated Polymer-Based Organic Solar Cells. *Chem. Rev.* **2007**, *107*, 1324−1338.
(63) Cowan, S. R.; Banerji, N.; Leong, W. L.; Heeger, A. J. Charge Formation, Recombination, and Sweep-Out Dynamics in Organic Solar Cells. *Adv. Funct. Mater.* **2012**, *22*, 1116−1128.
(64) Sforazzini, G.; Orentas, E.; Bolag, A.; Sakai, N.; Matile, S. Toward Oriented Surface Architectures with Three Coaxial Charge-Transporting Pathways. *J. Am. Chem. Soc.* **2013**, *135*, 12082−12090.
(65) Charbonnaz, P.; Zhao, Y.; Turdean, R.; Lascano, S.; Sakai, N.; Matile, S. Surface Architectures Built around Perylenediimide Stacks. *Chem.—Eur. J.* **2014**, *20*, 17143−17151.
(66) Bolag, A.; López-Andarias, J.; Lascano, S.; Soleimanpour, S.; Atienza, C.; Sakai, N.; Martín, N.; Matile, S. A Collection of Fullerenes for Synthetic Access Toward Oriented Charge-Transfer Cascades in Triple-Channel Photosystems. *Angew. Chem., Int. Ed.* **2014**, *53*, 4890−4895.

DOI: 10.1021/acs.jpcc.5b04060
J. Phys. Chem. C 2015, 119, 14999−15008